# Imprint of the speed of sound in nuclear matter on global properties of neutron stars

Na Zhang, Dehua Wen,* and Houyuan Chen
*School of Physics and Optoelectronics, South China University of Technology, Guangzhou 510641, People's Republic of China*

(Received 3 September 2018; revised manuscript received 9 December 2018; published 15 March 2019)

Internal structure and macroscopic properties of neutron stars are strongly correlated with the equation of state (EOS) of dense matter, while the EOS remains exceedingly uncertain especially at high densities. The observed massive neutron star with gravitation mass of $\approx 2\,M_\odot$ have imposed strong constraints on the EOS of super-dense matter. The upper limit of the speed of sound, as a crucial quantity to characterize the stiffness of the EOS, has significant influence on the maximum mass of a neutron star. The main propose of this work is to probe the possible lower bound for the upper limit of the speed of sound, where being coincident with the observations for massive neutron stars is considered. By employing a set of heterogeneous EOSs and through a constructed EOS model to describe the high-density part of the employed EOSs, we conclude that the upper limit of the speed of sound can be as low as 0.5386 $c$ (where $c$ is the speed of light). Furthermore, to eliminate the effect of the model dependence for the EOSs, we adopt a set of parameterized and model-independent EOSs to investigate this problem. As a result, a lower bound 0.5749 $c$ of the upper limit of the speed of sound is obtained, which is very close to the free-quark-matter's speed of sound, $\frac{1}{\sqrt{3}}c$. In addition, we semiempirically analyze the characteristics of the profile of neutron star $M$-$R$ relations and find out that the profiles of $M$-$R$ relations mainly depend on the speed of sound of the central density of neutron star sequences in the mass range around 0.3 to $1\,M_\odot$. However, the $M$-$R$ profile also can be explained by the universal relation proposed by Lattimer *et al.* Astroph. J. **550**, 426 (2001), where the case with extremely soft EOS in $\rho_0$ to $2\rho_0$ should be excluded.

DOI: 10.1103/PhysRevC.99.035803

## I. INTRODUCTION

As a natural laboratory for the study of dense matter, neutron stars (NSs) have drawn much attention from various research fields, including nuclear physics, astrophysics, particle physics, etc. In the hydrostatic equilibrium case, the global stellar properties of a nonrotating NS, including the observable mass ($M$) and radius ($R$) of NS, can be determined by the Tolman-Oppenheimer-Volkoff (TOV) equations [1,2] once the equation of state (EOS) is supplied. Unfortunately, the EOS of the super dense nuclear matter is not determined very well currently. The primary reason lies in the deficient understandings of the isospin dependence of nuclear-nuclear interaction and the nature of multibody problems [3–7].

Fortunately, the observations of massive NSs have imposed strong constraints on the EOS of super-dense matter (see also the references about the NS mass distribution [8,9]). In astronomical observation, the number of NSs with accurate measurements in binary systems is rapidly increasing due to development in relevant techniques and instruments. At present, there are 35 individual pulsars having precise determinations in mass in the range of 1.17–2.01 $M_\odot$ [10], in which the most massive one is $J0348+0432$ with gravitational mass of $2.01 \pm 0.04\,M_\odot$ [11].

The accurate determination of the maximum mass of NS is of great concern in the study of astrophysics [12], because it helps identify whether an observed massive object is a NS or a black hole. While in nuclear theory, the EOS that cannot support the observed maximum mass of NS will be excluded. In the aspects of theoretical sense, many efforts have been made on giving the maximum mass of NSs [13–15]. For example, Rhoades and Ruffini provided an estimation of maximum mass for nonrotating NS as $M_{\max} \leqslant 3.2\,M_\odot$ by using variational techniques [16]. However, the observation of GW 170817 has opened a new window in understanding the maximum mass of NS. In the past year, by using the observational data of GW 170817, great efforts have been made in constraining the maximum mass [17–19]. For example, by combining the electromagnetic and gravitational wave information from the GW170817, an upper limit of maximum mass $\leqslant 2.17 M_\odot$ is placed at 90% confidence level [17].

The maximum mass of NS depends strongly on the EOS of $\beta$-stable nuclear matter [20–23]. Normally, a stiffer EOS will support a higher maximum mass of neutron star [24]. The speed of sound of dense matter, defined as $v_s = c(\frac{dp}{d\rho})^{\frac{1}{2}}$ (where $c$ is the speed of light, $p$ is the pressure, and $\rho$ is the energy density), is an important parameter to describe the stiffness and incompressibility of EOS for dense matter. As early as the 1960s, scientist realized that at ultrahigh densities the speed of sound will be very high and can be up to the speed of light [25], even exceed the speed of light [26]. As we know, limited by the principle of causality (a detailed discussion about the causality in dense matter please refer to Ref. [27]), the speed of sound within the star should not exceed the speed of light [16,28]. Therefore, the speed of light

*wendehua@scut.edu.cn

 

places an absolute upper limit on the speed of sound. Can the speed of sound in neutron star be sure as high as the speed of light? Many of the researchers believe that the speed of sound in NS cannot reach such a high speed [12,29,32,33]. Lattimer have argued that the causal limit is too extreme theoretically because the highly compressed hadronic matter may convert asymptotically to free quark matter where the speed of sound is $v_s = c/\sqrt{3}$ [29]. Interestingly, based on the observation of the massive neutron star ($\approx 2.0 M_\odot$) and specific EOSs, two recent works declare that there is an irreconcilable contradiction between the upper limit of sound velocity $v_s = c/\sqrt{3}$ and the massive neutron star observation [30,31]. In fact, to place the upper limit of the speed of sound in neutron star comes to be an essential research in both nuclear theory and astrophysics related compact stars. For example, based on the model-dependent EOSs and the observation of massive neutron star, Tews *et al.* argued that the speed of sound should reach values closer to the speed of light at a few times of the nuclear saturation density [33]. And based on a flexible piecewise polytropic equation of state model, Alsing *et al.* obtained a lower bound on the maximum speed of sound $v_s^{\max} > 0.63c$ (99.8%) inside the neutron star, where the Gaussian mass likelihoods and Bayesian parameter inference are employed to determine the maximum mass of neutron star [32].

To sum up, the determination of maximum speed of sound in neutron star is extraordinarily important in both understanding the property of NS and constraining EOS of dense matter. In this paper, we will discuss the influence of the speed of sound on the $M$-$R$ relation first, and we will try to understand the characteristics of the profile of neutron star $M$-$R$ relation by the speed of sound. And then we construct a set of EOS models describing the high-density part of the employed EOSs and further investigate the possible lower upper limit of the speed of sound. Furthermore, to eliminate the effect of the model dependence for the EOSs, we will employ the parameterized and model-independent EOSs reinvestigating the same question.

The paper is organized as follows. The influences of the speed of sound on the global properties of neutron stars are discussed in Sec. II, including a qualitative discussion on both maximum mass and M-R profile. We probe the possible lower bound for upper limit of the speed of sound in Sec. III. Conclusions are given in Sec. IV.

## II. THE EFFECT OF THE SPEED OF SOUND ON THE GLOBAL PROPERTIES OF NS

To qualitatively demonstrate the effects of constraining the speed of sound, we adopt several EoS models for neutron star. They are: (1) APR EOS [34], (2) DBHF EOS [35], (3) SLY4 EOS [36], (4) L25 and L45 EOS [37], and (5) Soft and Stiff EOSs [24]. The APR EOS adopts variational chain summation methods and considered the new Argonne 18 two-nucleon interaction, which provides an excellent fit to all of the nucleon-nucleon scattering data in the Nijmegen database [34]. The DBHF EOS employs the Dirac equation for single-particle motion in nuclear matter, and the nucleon wave function is obtained self-consistently. Actually, the description of the nucleon motion in nuclear matter with a Dirac spinor can be regarded as effective many-body force contributions [35]. The SLY4 EOS is based on the Skyrme-Lyon effective nucleon-nucleon interactions with a new set of improved parameters which can reproduce the experimental data of the day very well [36,38]. L25 EOS and L45 EOS take a range of the slope of the symmetry energy $L$ from model analysis of terrestrial nuclear laboratory experiments coupled with the theoretical calculations of pure neutron matter [37]. Hebeler *et al.* constructed a couple of EOSs, and among them Stiff EOS and Soft EOS are separately possible stiffest and softest EOSs under the constraint of causality and their models [24]. For more details on the EOSs please refer to the corresponding references.

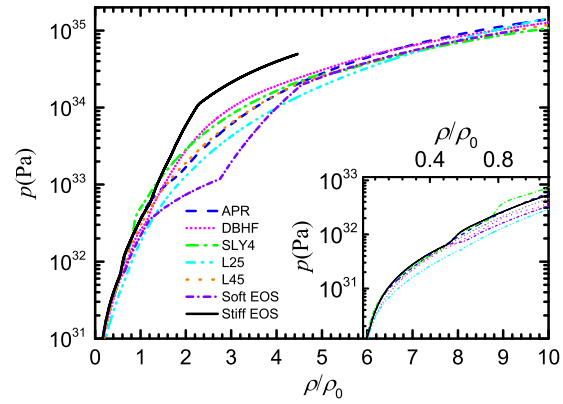


FIG. 1. Pressure-density relation for the EOSs. The inset shows details of these EOSs at $\rho < \rho_0$, where the nuclear saturation density $\rho_0 = 2.7 \times 10^{17}\,\mathrm{kg\,m^{-3}}$.

The adopted EOSs are presented in Fig. 1. It is shown that among the adopted EOSs there is a remarkable disparity in the supranuclear density region. It is clear that at the higher density region, the Stiff EOS is the stiffest one, while the Soft EOS is the softest one (in the density region $\approx 1\,\rho_0$ to $4\,\rho_0$). As for L25 EOS and APR EOS, they are also relatively soft in this region. Nevertheless, the stiffness at higher density is different, APR EOS is the stiffest one in the density region from $\approx 6.5\,\rho_0$ to $9\,\rho_0$, while L25 EOS at exceedingly high density (above $9\,\rho_0$) becomes the stiffest one. In fact, such differences among nuclear EOSs will have dramatic effects on the maximum mass configuration of NS. However, EOSs at density lower than $\rho_0$ also have small differences, as shown in the inset of Fig. 1. Fortunately, EOS in this region only has negligible contribution to the maximum mass.

For a static and spherical symmetric compact star, the hydrostatic equilibrium equations were first deduced from Einstein's equations by Tolman *et al.*, also named TOV equations [1,2]:

$$\begin{aligned} \frac{dp}{dr} &= -\frac{(p+\rho)[m(r)+4\pi r^3 p]}{r[r-2m(r)]}, \\ \frac{dm(r)}{dr} &= 4\pi r^2 \rho, \end{aligned} \tag{1}$$

where $m(r)$ is the mass within the given radius $r$, and the geometrical unit ($G = c = 1$) is adopted in these equations.

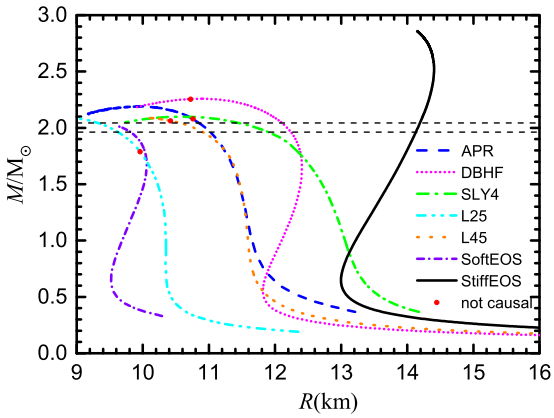


FIG. 2. The $M$-$R$ curves for EOSs demonstrated in Fig. 1. The red dots denote the maximum masses for the corresponding EOSs when causality is considered.

The TOV equations are integrated from the origin ($r = 0$, $\rho = \rho_c$) to the surface of the star ($r = R,\ p = 0$) when an EOS is given. From the function $m(r)$ and $p(r)$ obtained in this way, it is possible to determine any of the macroscopic properties of the NS. In this manner, an EOS generates a unique $M$-$R$ relation for NSs.

The $M$-$R$ profiles predicted by the adopted EOSs are displayed in Fig. 2. It is shown that the prediction for radius of a typical NS ($\approx 1.4\,M_\odot$) have a large uncertainty with a wide range of about 10.0–13.5 km. As pointed out by Ref. [39], the stellar radius is relevant to the pressure at vicinity of $2\,\rho_0$. Ignoring the constraint of the speed of sound for the EOSs, the $M$-$R$ relations are consistent with the massive neutron star observations [11], as shown in Fig. 2. For further analysis, the speed of sound as a function of density is plotted in Fig. 3. It is easier to see from the figure that most EOSs are not described by a single theoretic model. Generally, they are jointed with at least three parts: outer crust, inner crust, and core; see also

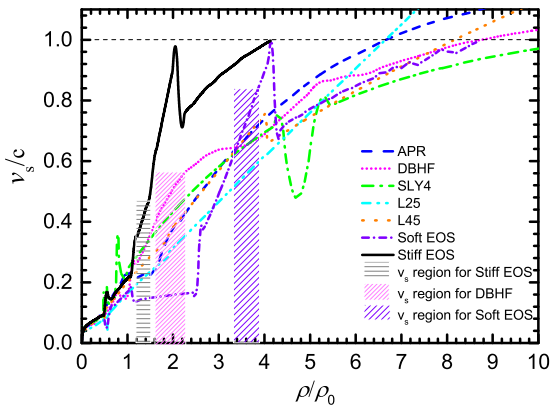


FIG. 3. The speed of sound as a function of the density for the EOSs, where the speed of sound is in units of speed of light $c$. The horizontal dash line denotes the speed of light as causality constraint at which several EOSs in the figure are truncated when causality is considered. The vertical bands from left to right indicate the speed of sound at central density of NS with mass of 0.3–1 $M_\odot$ under Stiff EOS, DBHF EOS, and Soft EOS, respectively.

TABLE I. Properties of most massive NS for some of the EOSs mentioned in Fig. 1, where $M_{\rm max}$ are the deduced maximum masses regardless of causality, and $M_{\rm causal}$ are the maximum masses considering the causality, where $\rho_{\rm causal}$ and $p_{\rm causal}$ are the corresponding central density and pressure, respectively.

| EOSs | $M_{\rm max}\ (M_\odot)$ | $M_{\rm causal}\ (M_\odot)$ | $\rho_{\rm causal}\ (\rho_0)$ | $p_{\rm causal}\ (10^{34}{\rm Pa})$ |
|---|---|---|---|---|
| APR | 2.1869 | 2.0820 | 6.6863 | 7.0015 |
| DBHF | 2.2559 | 2.2559 | 8.7688 | 11.4829 |
| L25 | 2.0920 | 1.7854 | 6.6748 | 5.5759 |
| L45 | 2.0914 | 2.0604 | 8.1854 | 9.0599 |

in Ref. [40]. The obvious jumps in the figure of the speed of sound are caused by the merger of EOS models for different segments.

Several EOSs shown in Fig. 3 are noncausal at high density. Obviously, an EOS that does not satisfy the law of causality is nonphysical. This feature will draw some effect on the value of the maximum mass of NS. The boundary that satisfies the law of causality is indicated in red point, as shown in Fig. 2 (see Table I for the exact data). It is shown that after considering the causality constraint, some of the maximum masses decrease more or less. For example, the reduction for APR EOS and L25 EOS are prominent, and that for DBHF EOS and L45 EOS are not significant. Generally, causality constraint will not violate the accordance with observations of massive neutron star, except for L25 EOS. According to the implication of causality on the maximum mass configuration of NS, it is deduced that the well-known and fundamental constraint condition (causality) has imposed certain but not strict enough constraint on the upper limit of the speed of sound in neutron stars.

There is another interesting phenomenon worth noting, that is, the profiles of $M$-$R$ relations of NSs displayed in Fig. 2 can be simply divided into two types: (1) The stellar radius decreases monotonously with the increase of stellar mass in the whole sequence, where the EOSs include the APR, SLY4, L25, and L45. (2) Beginning from $\approx 0.5\,M_\odot$, the stellar radius increases with the growth of stellar mass, where the EOSs include the DBHF, Soft and Stiff. Nevertheless, all of the NS sequences are still stable, as they satisfy the stellar stable condition $\partial M(\rho_c)/\partial\rho_c > 0$, as shown in Fig. 4. It is well-known that the behavior of EOS has the decisive effect on the properties of NS. We speculate that the speed of sound for NS EOS may provide clue to explain the different characteristics among the $M$-$R$ profiles yielded by the EOSs above. To further the discussion, we present the profile of gravitational mass versus the speed of sound at central density in Fig. 5. It seems that the speed of sound at stellar center, with respect to the mass range of 0.3–1 $M_\odot$, is relatively higher for the second catalog of EOSs in Fig. 2.

As shown in Fig. 5, the speeds of sound of the central density for the EOSs (DBHF, Soft, and Stiff) at the stellar mass region around 0.3–1 $M_\odot$ are comparatively large and grow rapidly. We suspect that the divergence of the speed of sound leads to the different types of $M$-$R$ relations. To further demonstrate this speculation, we select the Soft EOS as a

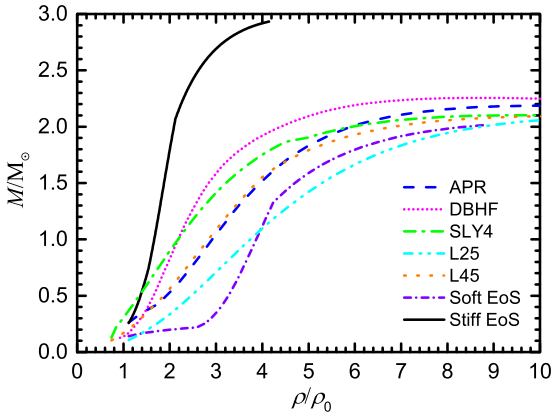


FIG. 4. The stellar masses as a function of the central densities for the adopted EOSs.

sample to investigate the influence on the $M$-$R$ profile by the speed of sound. We enlarge or diminish the speed of sound through modifying the stiffness of Soft EOS. Through piecewise modifying of the speed of sound for the NS sequences, we investigate the effects on the profiles of the $M$-$R$ relations by the speed of sound of the central densities. The results are plotted in Fig. 6, where the left panel presents the $M$-$R$ relations yielded by the modified EOSs, and the right panel shows the modified EOSs (the inset) and the speed of sound at central density versus the corresponding stellar mass. It is shown that only when the speed of sound at mass regions of about 0.3–1 $M_\odot$ is changed to some degree, would the shape of $M$-$R$ profile transform prominently. We also investigate the situation of other EOSs in this manner, and a similar result is obtained. We qualitatively understand this consequence as follow: as the radius increases with the increase of mass, the speed of sound at central density corresponding to 0.5 $M_\odot$ begins to rise, forming a heavier core for the neutron star to balance the gravity, and thus reducing the radius through the contraction with the increase gravity. Based on discussion above, we argue that the $M$-$R$ relation profile of NS mainly depends on the speed of sound at the central density with respect to the gravitational mass of 0.3–1 $M_\odot$.

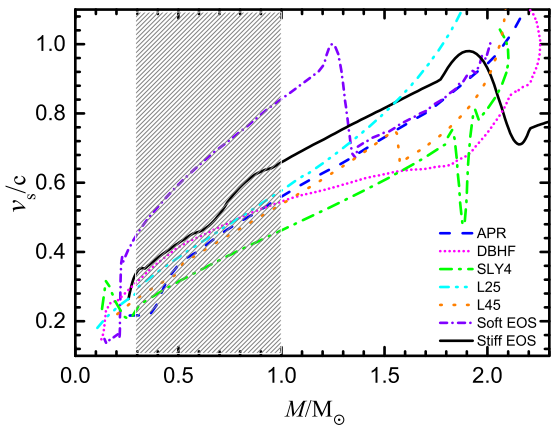


FIG. 5. The relations between the stellar mass and speed of sound of the central density for the corresponding NS sequences.

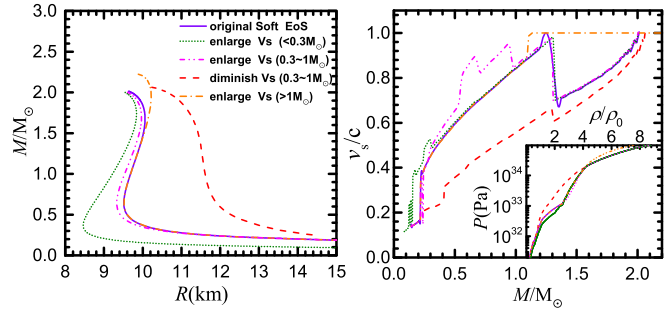


FIG. 6. Left panel: the $M$-$R$ relation profiles reproduced by the Soft EOS without modification and with piecewise modification on the speed of sound. Right panel: the speed of sound at central density $\rho_c$ vs. the stellar mass for EOSs mentioned in the left, where the inset is the $p$-$\rho$ relations of the modified EOSs. The legend is the same for both plots.

Moreover, the universal relation proposed by Lattimer *et al.* [39] provides another way to understand the characteristics of the profile of NS's $M$-$R$ relation. The universal relation is expressed as follows:

$$C(n, M) \cong R_M P_n^{-\frac{1}{4}}, \tag{2}$$

where $R_M$ is stellar radius with respect to the given gravitational mass $M$, and $P_n$ is pressure at the given baryon density $n$. As has been pointed out in Ref. [39], this universal relation is not suitable for the case when the EOS becomes extremely soft in $\rho_0$–$2\rho_0$. To understand this universal relationship further, we studied dozens of equations of state and calculated the quantity $C(n, M)$. We note that this quality is definitely associated with the $n$ and $M$. It is clear that the quantity $C$ is related to two degrees of freedom, $n$ and $M$. To minimize the uncertainty of $C(n, M)$, we try to find the specified relation $n(M)$ first. Satisfactorily, this specified relation $n(M)$ does exist. The optimization of $n(M)$ relation is plotted in Fig. 7. This $n(M)$ relation ensures the best universality of Eq. (2).

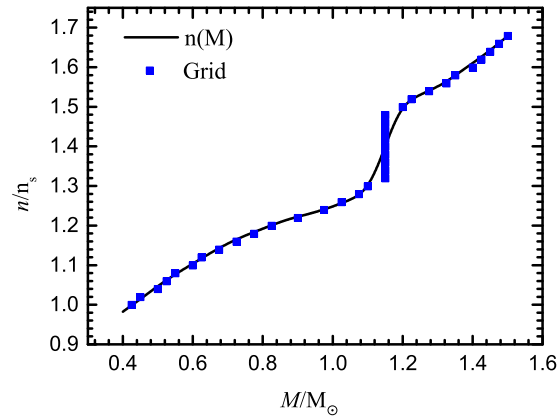


FIG. 7. The $n(M)$ relation, where the squares are the minimal deviation of $C(n, M)$ found in the original computation grid and the solid line is the smooth approximation of $n(M)$ estimated from the scatters. To obtain this relation, the $C[n(M), M]$ is assured having the best universality at each stellar mass.

TABLE II. The quantity $C_n$ in the units of km fm$^{3/4}$ MeV$^{-1/4}$ with respect to the given gravitational mass $M$ in the units of $M_\odot$.

| | | | | | | | | | | | | | | | |
|---|---|---|---|---|---|---|---|---|---|---|---|---|---|---|---|
| $M$ | 0.52 | 0.54 | 0.56 | 0.58 | 0.60 | 0.62 | 0.64 | 0.66 | 0.68 | 0.70 | 0.72 | 0.74 | 0.76 | 0.78 | 0.80 |
| $C_n$ | 9.50 | 9.39 | 9.30 | 9.21 | 9.13 | 9.06 | 8.98 | 8.92 | 8.86 | 8.80 | 8.75 | 8.70 | 8.66 | 8.62 | 8.58 |
| $M$ | 0.82 | 0.84 | 0.86 | 0.88 | 0.90 | 0.92 | 0.94 | 0.96 | 0.98 | 1.00 | 1.02 | 1.04 | 1.06 | 1.08 | 1.10 |
| $C_n$ | 8.54 | 8.51 | 8.47 | 8.45 | 8.43 | 8.40 | 8.38 | 8.35 | 8.33 | 8.30 | 8.27 | 8.24 | 8.20 | 8.14 | 8.05 |
| $M$ | 1.12 | 1.14 | 1.16 | 1.18 | 1.20 | 1.22 | 1.24 | 1.26 | 1.28 | 1.30 | 1.32 | 1.34 | 1.36 | 1.38 | 1.40 |
| $C_n$ | 7.91 | 7.73 | 7.55 | 7.39 | 7.27 | 7.21 | 7.17 | 7.14 | 7.11 | 7.08 | 7.04 | 7.00 | 6.96 | 6.92 | 6.88 |

According to the unique path of $n(M)$, the coefficient in Eq. (2) could be written as $C(n, M) = C_n(M)$, and the calculation results of $C_n(M)$ are presented in Table II. Then we can get the derivative of radius with respect to the mass as

$$\frac{dR_M}{dM} = P_n^{\frac{1}{4}}\left(\frac{dC_n}{dM} + \frac{1}{4}\frac{C_n}{P_n}\frac{dn}{dM}\frac{dP_n}{dn}\right), \tag{3}$$

where $dn/dM$ is determined by the path of $n(M)$, and the $dC_n/dM$ is obtained from the tabular $C_n(M)$, while both $dP_n/dn$ and $P_n$ could be interpolated from the EOSs. Thus, we can numerically calculate $dR_M/dM$, and the results are presented in Table III. It is shown that for the seven EoSs, excluding the Soft EOS (extremely soft in the density region $\rho_0$–$2\rho_0$), the characteristics of the $M$-$R$ profile is consistent with the $dR_M/dM$ extracted from the universal relation of Eq. (2).

## III. THE LOWEST UPPER LIMIT OF THE SPEED OF SOUND

One of the motivations of this work is to inversely constrain the upper limit of the speed of sound by considering the astronomical observation. To probe the lowest upper limit of the speed of sound, we hypothesize a speed of sound $v_c$ as the theoretical value for the upper limit of the speed of sound. We subsequently construct a maximum mass configuration by employing the following constructed EOS:

$$\begin{aligned} &\text{nuclear EOS}, \ \ \rho < \rho_{\rm crit};\\ &p = v_c^2(\rho - \rho_{\rm crit}) + p_{\rm crit}, \ \rho \geqslant \rho_{\rm crit}. \end{aligned} \tag{4}$$

According to Eq. (4), the EOS is divided into two regions. In the region of density less than the critical density $\rho_{\rm crit}$, the original nuclear EOS presented in Fig. 1 is employed. It is clear that the constructed EOSs can automatically guarantee the continuity of the speed of sound at $\rho_{\rm crit}$. As in the region above $\rho_{\rm crit}$, the pressure is extended in the form of $p = v_c^2(\rho - \rho_{\rm crit}) + p_{\rm crit}$, it is easy to understand that the EOS was softened at high density comparing with the original EOS. Normally, the constructed EOSs only modify the EOSs at relatively high densities ($>1.5\rho_0$), as shown in Table IV,while at low density region the constructed EOS remains the same data from its original EoS.

We obtain the unique minimum value of the upper limit of the speed of sound $v_{\rm min}$ for the constructed EOSs in the following way. To an constructed EOS, we first adopt a relatively higher value for $\rho_{\rm crit}$, where the speed of sound at this density is denoted as $v_s$. Then we can get a maximum stellar mass by the constructed EOS with the adopted $\rho_{\rm crit}$ and the corresponding $v_s$. As we continuously decrease the $\rho_{\rm crit}$, we will finally obtain a lowest quantity for $v_s$ (denoted as $v_{\rm min}$) that corresponds to $M = 2.01M_\odot$. At this $\rho_{\rm crit}$, the corresponding $v_c$ is just the unique $v_{\rm min}$ to support the precisely observed maximum mass $M = 2.01M_\odot$ by the constructed EOS. It is worth pointing out that for those EOSs with the speed of sound not increasing monotonically with density (such as the SLY4, Stiff, and Soft EOSs, as shown in Fig. 3), the speed of sound $v_c$ at $\rho_{\rm crit}$ may be smaller than the speed of sound $v_c$ at a lower density. In this case, we need to synchronously modify the EOSs at the lower density part in the same way.

The minimum possible values for the upper limit of the speed of sound for the adopted EOSs are presented in Table IV. It is shown that the values of $v_{\rm min}$ for various nuclear EOSs lie between the two extreme cases: (1) The minimum limit with value of $0.5386\,c$ for Stiff EOS, which is even less than the speed of sound for free quark matter EOS with the value of $c/\sqrt{3}$. (2) The extremely high limit with value of light speed $c$ for Soft EOS and L25 EOS. As shown in Table IV, the possible lowest values for the upper limit of the speed of sound $v_{\rm min}$ deduced from Stiff, DBHF, and SLY4 EOSs, are

TABLE III. The quantity of $P_n$, $dP_n/dn$, and $dR/dM$ at $M = 1.0\,M_\odot$.

| EOSs | $P_n$ (MeV fm$^{-3}$) | $dP_n/dn$ (MeV) | $dR/dM$ (km $M_\odot^{-1}$) |
|---|---|---|---|
| APR | 5.0245 | 50.5362 | − 0.53827 |
| DBHF | 4.6332 | 87.1611 | 0.3281 |
| SLY4 | 7.0306 | 97.1336 | − 0.1778 |
| L25 | 2.9663 | 45.1035 | − 0.0218 |
| L45 | 4.5573 | 66.3625 | − 0.0869 |
| Soft EOS | 2.7253 | 21.5545 | − 0.6458 |
| Stiff EOS | 6.8819 | 159.4117 | 0.8317 |

TABLE IV. The minimum possible values for the upper bounds of sound speed for the adopted EOSs supporting the mass observational constraints.

| EOSs | $v_{\rm min}(c)$ | $\rho_{\rm crit}(\rho_0)$ | $p_{\rm crit}(10^{34}Pa)$ | $\rho_c(\rho_0)$ |
|---|---|---|---|---|
| APR | 0.7381 | 3.9974 | 1.8315 | 9.6577 |
| DBHF | 0.5934 | 2.5161 | 0.7538 | 7.5007 |
| SLY4 | 0.6233 | 4.4618 | 2.5533 | 8.1629 |
| L25 | 1.0030 | 6.6748 | 5.5759 | 12.0911 |
| L45 | 0.7275 | 3.8611 | 1.6735 | 9.5022 |
| Soft EOS | 1.0000 | 8.8807 | 10.6020 | 8.8807 |
| Stiff EOS | 0.5386 | 1.5350 | 0.2291 | 4.1414 |

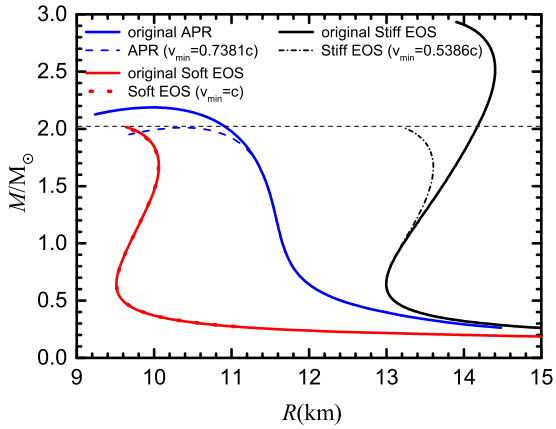


FIG. 8. Effects on the mass-radius curves for three representative EOSs by the sound speed limitation. Solid lines are computed with the original EOSs (ignoring any constraint of the sound speed). Dash lines are obtained by the constructed EOSs with $v_{\rm min}$ supporting $M_{\rm max} = 2.01 M_\odot$.

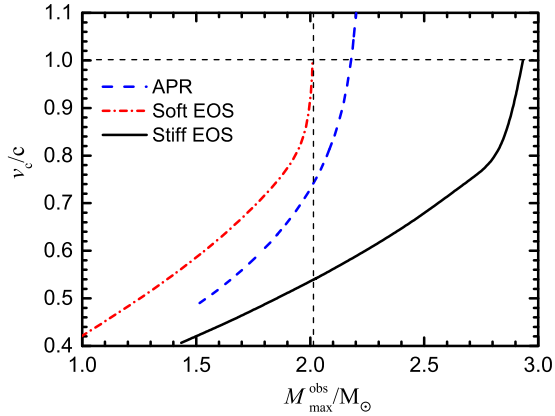


FIG. 9. The dependence of the lower upper limit of sound speed $v_{\rm min}$ on the maximum observational mass $M_{\rm max}$.

comparatively small (around 0.6 $c$), and their corresponding critical densities are also lower, but for Soft EOS and L25 EOS, they have extremely high upper limit of the speed of sound. What has made such a significant difference on the $v_{\rm min}$ for these adopted EOSs? We can seek the answer in Figs. 1 and 3. It is clear that the former kinds of EOSs are relatively stiffer at density below about 4 $\rho_0$, as shown in Fig. 1, and these EOSs also have relatively higher sound speeds at densities below about 3 $\rho_0$, as shown in Fig. 3.

To further clarify the maximum mass dependence on the upper limit of the speed of sound, we select three typical EOSs (APR, Soft, and Stiff) as samples for the next analysis. The $M$-$R$ relations yielded by their original EOSs and the constructed EOSs (with $\rho_{\rm crit}$ at their minimum upper limit of the speed of sound $v_{\rm min}$) are displayed in Fig. 8, respectively. It is shown that the impact of the upper limit of the speed of sound on the maximum mass is prominent (with the exception of Soft EOS, which was constructed by Hebeler *et al.* with the consideration of causality, and since its $v_{\rm min}$ is equal to the speed of light, it results to the coincidence of two curves). It is clear that the EOS with a lower $v_{\rm min}$ can support a higher maximum mass. For the typical example of Stiff EOS with $v_{\rm min} = 0.5386\,c$, it yields the NS with the maximum mass as large as $2.9\,M_\odot$.

It is easy to understand that the lowest upper limit of the speed of sound $v_{\rm min}$ will strongly depend on the value of the observed maximum mass $M^{\rm obs}_{\rm max}$ of NS. If a more massive neutron star (with mass larger than $2.01\,M_\odot$) is observed, then the lowest upper limit of the speed of sound $v_{\rm min}$ will increase correspondingly. To show this point more clearly, we display the dependency of the $v_{\rm min}$ on the $M^{\rm obs}_{\rm max}$ in Fig. 9. It is clear that a higher upper limit of the speed of sound is needed if a more massive NS is observed in the future.

The discussion above is based on a set of model-dependent EOSs. To eliminate the effect of the model dependence for the EOSs, we employ the parameterized and model-independent EOSs to probe the possible lowest upper limit of the speed of sound. The following is a brief introduction to the parameterized and model-independent EOSs.

The nucleon specific energy $E(\rho, \delta)$ can be well approximated by the empirical parabolic law as [41,42]

$$E(\rho, \delta) = E_0(\rho) + E_{\rm sym}(\rho)\delta^2 + O(\delta^4), \tag{5}$$

where $E_0(\rho)$ is the energy per nucleon of symmetric nuclear matter, $E_{\rm sym}(\rho)$ is the symmetry energy of asymmetric nuclear matter and $\delta$ is the isospin asymmetry, defined as $\delta = (\rho_n - \rho_p)/\rho$, in which $\rho_n$ and $\rho_p$ are the number densities of neutron and proton, respectively, and $\rho = \rho_n + \rho_p$. Considering the fact that the equation of state of the neutron-rich asymmetric nuclear matter is still not determined very well, it is helpful to parametrize the expansion coefficients first, that is [43]

$$E_0(\rho) = E_0(\rho_0) + \frac{K_0}{2}\left(\frac{\rho-\rho_0}{3\rho_0}\right)^2 + \frac{J_0}{6}\left(\frac{\rho-\rho_0}{3\rho_0}\right)^3, \tag{6}$$

$$E_{\rm sym}(\rho) = E_{\rm sym}(\rho_0) + L\left(\frac{\rho-\rho_0}{3\rho_0}\right) + \frac{K_{\rm sym}}{2}\left(\frac{\rho-\rho_0}{3\rho_0}\right)^2 + \frac{J_{\rm sym}}{6}\left(\frac{\rho-\rho_0}{3\rho_0}\right)^3, \tag{7}$$

where $\rho_0 = 2.7 \times 10^{17}\,{\rm kg\,m^{-3}}$ is the nuclear saturation density. According to the existing knowledge on the parameters at saturation density, the most probable values of them are as follows: $K_0 = 230 \pm 20\,{\rm MeV}$, $E_{\rm sym}(\rho_0) = 31.7 \pm 3.2\,{\rm MeV}$, $L = 58.7 \pm 28.1\,{\rm MeV}$, and $-300 \leqslant J_0 \leqslant 400\,{\rm MeV}$, $-400 \leqslant K_{\rm sym} \leqslant 100\,{\rm MeV}$, $-200 \leqslant J_{\rm sym} \leqslant 800\,{\rm MeV}$. It is worth noting that the Taylor expansions will become increasingly inaccurate as the density gradually deviates from the saturation density and do not converge when $\rho > 1.5\rho_0$. At the high-density region, the parameters $J_0$, $K_{\rm sym}$, and $J_{\rm sym}$ are no longer to be the Taylor expansion coefficients but the free parameters expecting to be resolved by the future astronomy observations [43].

In the above parameter space, we generate about 100 000 EOSs to seek the lowest upper limit of the speed of sound. It should be pointed out that here we directly use the generated EOSs and do not construct the EOSs at the high-density part as Eq. (4). The corresponding results are presented in Fig. 10.

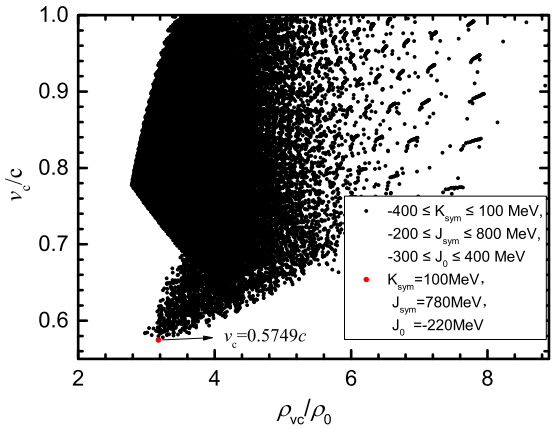


FIG. 10. The scatter diagram of the lower upper limits of the speed of sound vs. the corresponding central densities, where the lower upper limits of the speed of sound of all the trial EOSs are obtained by meeting the requirement to support the maximum stellar mass 2.01 $M_\odot$. The red point at the bottom of the graph denotes the lowest upper limit of the speed of sound among the tens of thousands of EOSs, where the values of the corresponding parameters $K_{\rm sym}$, $J_{\rm sym}$, and $J_0$ of this point are shown in the legend (beside the red point). The parameter spaces of $K_{\rm sym}$, $J_{\rm sym}$, and $J_0$ are also labeled in the legend (beside the black point).

In this manner, a lower limit 0.5749 $c$ of the upper limit of the speed of sound is obtained. Unexpectedly, this lower limit is coincidentally very close to $\frac{1}{\sqrt{3}}c$, the well-known upper limit of the speed of sound deduced from free quark matter [29]. We are not sure if there is a physical connection of this coincidence.

## IV. CONCLUSIONS

We investigate the effect of the speed of sound on the global properties of NSs. First, we recheck the basic requirement, that is, the causality condition $v_s \leqslant c$ for the adopted EOSs. It is shown that the condition $v_s \leqslant c$ reduces the maximum mass of NSs for a class of nuclear models (such as L25 and APR EOSs). We found that the tendency of $M$-$R$ relation mainly depends on the speed of sound at the corresponding central density for NSs within 0.3–1 $M_\odot$. This conclusion is also analyzed with a semiempirical formula that derived from the universal relation found by Lattimer *et al.* [39]; however, the EOSs which are extremely soft in $\rho_0$–$2\rho_0$ violate this rule.

We adopt the precisely observed maximum stellar mass 2.01 $M_\odot$ as a fundamental requirement to set the lower upper limit of the speed of sound. By employing a constructed model to describe the high density part of EOSs, the lowest quantity for the upper bound of the speed of sound in the interior of neutron star is investigated among a heterogeneous set of EOSs. As a result, it is found that the Stiff EOS holds the lowest value ($v_{\rm min} = 0.5386\,c$) for the upper bound of the speed of sound. Furthermore, to eliminate the effect of the model dependence for the EOSs, we use a parameterized and model-independent EOS model to investigate this problem, where the parameters of EOSs are constrained by the terrestrial experiment. We obtain a lower bound 0.5749 $c$ for the upper limit of the speed of sound, which is very close to $\frac{1}{\sqrt{3}}c$, the speed of sound of free quark matter [29]. Moreover, we also probe the relation between the lower upper limit of the speed of sound and the maximum observed stellar mass, and it is shown that there is a strong dependence of the lower upper limit of the speed of sound on the maximum observed stellar mass. Obviously, if a more massive NS is observed in the future, a higher lower upper limit of the speed of sound should be needed.

## ACKNOWLEDGMENTS

We thank Bao-An Li for helpful discussions and the referee for helpful comments and suggestions. This work is supported by NSFC (Grants No. 11275073, No. 11675226, and No. 11722546) and the talent program of South China University of Technology (Grant No. K5180470). This project has made use of NASA's Astrophysics Data System.

[1] R. C. Tolman, Phys. Rev. **55**, 364 (1939).
[2] J. R. Oppenheimer and G. M. Volkoff, Phys. Rev. **55**, 374 (1939).
[3] S. Weinberg, Phys. Lett. B **251**, 288 (1990).
[4] S. Weinberg, Nucl. Phys. B **363**, 3 (1991).
[5] H. Heiselberg and V. Pandharipande, Ann. Rev. Nucl. Particle Sci. **50**, 481 (2000).
[6] K. Hebeler and A. Schwenk, Phys. Rev. C **82**, 014314 (2010).
[7] Z. Q. Feng, Nucl. Sci. Tech. **29**, 40 (2018).
[8] B. Kiziltan, A. Kottas, M. D. Yoreo, and S. E. Thorsett, Astrophys. J. **778**, 66 (2013).
[9] M. C. Miller and J. M. Miller, Phys. Rep. **548**, 1 (2015).
[10] F. Ozel and P. Freire, Ann. Rev. Astron. Astrophys. **54**, 401 (2016).
[11] J. Antoniadis, P. C. Freire, N. Wex, T. M. Tauris, and R. S. Lynch, Science **340**, 1233232 (2013).
[12] J. B. Hartle, Phys. Rep. **46**, 201 (1978).
[13] V. Kalogera and G. Baym, Astrophys. J. **470**, L61 (1996).
[14] S. Lawrence, J. G. Tervala, P. F. Bedaque, and M. C. Miller, Astrophys. J. **808**, 186 (2015).
[15] C. L. Fryer, K. Belczynski, E. Ramirezruiz, S. Rosswog, G. Shen, and A. W. Steiner, Astrophys. J. **812**, 24 (2015).
[16] C. E. Rhoades and R. Ruffini, Phys. Rev. Lett. **32**, 324 (1974).
[17] B. Margalit and B. D. Metzger, Astrophys. J. Lett. **850**, L19 (2017).
[18] L. Rezzolla, E. R. Most, and L. R. Weih, Astrophys. J. Lett. **852**, L25 (2018).
[19] M. Ruiz, S. L. Shapiro, and A. Tsokaros, Phys. Rev. D **97**, 021501 (2018).
[20] S. L. Shapiro and S. A. Teukolsky, *Black Holes, White Dwarfs, and Neutron Stars* (John Wiley and Sons, New York, 1983).
[21] N. K. Glendenning, *Compact Stars: Nuclear Physics, Particle Physics, and General Relativity* (Springer, Berlin, 2000).

[22] P. Haensel, A. Y. Potekhin, and D. G. Yakovlev, *Neutron Stars 1: Equation of State and Structure* (Springer-Verlag, New York, 2007).
[23] S. Weinberg, in *Gravitational and Cosmology: Principle and Applications of the General Theory of Relativity* (Wiley, New York, 1972).
[24] K. Hebeler, J. M. Lattimer, C. J. Pethick, and A. Schwenk, Astrophys. J. **773**, 11 (2013).
[25] Ya. B. Zel'dovich, J. Exptl. Theoret. Phys. (U.S.S.R.) **41**, 1609 (1961) [Sov. Phys. JETP **14**, 1143 (1962)].
[26] S. A. Bludman and M. A. Ruderman, Phys. Rev. **170**, 1176 (1968).
[27] B. D. Keister and W. N. Polyzou, Phys. Rev. C **54**, 2023 (1996).
[28] E. Krotscheck and W. Kundt, Commun. Math. Phys. **60**, 171 (1978).
[29] J. M. Lattimer, *Astrophysics and Cosmology: Proceedings of the 26th Solvay Conference on Physics* (World Scientific, Singapore, 2014).
[30] P. F. Bedaque and A. W. Steiner, Phys. Rev. Lett. **114**, 031103 (2015).
[31] C. C. Moustakidis, T. Gaitanos, C. Margaritis, and G. A. Lalazissis, Phys. Rev. C **95**, 045801 (2017).
[32] J. Alsing, H. O. Silva, and E. Berti, MNRAS **478**, 1377 (2018).
[33] I. Tews, J. Carlson, S. Gandolfi, and S. Reddy, Astroph. J. **860**, 149 (2018).
[34] A. Akmal, V. R. Pandharipande, and D. G. Ravenhall, Phys. Rev. C **58**, 1804 (1998).
[35] P. G. Krastev and F. Sammarruca, Phys. Rev. C **74**, 025808 (2006).
[36] F. Douchin and P. Haensel, Astron. Astrophys. **380**, 151 (2001).
[37] D. H. Wen, W. G. Newton, and B. A. Li, Phys. Rev. C **85**, 025801 (2012).
[38] E. Chabanat, P. Bonche, P. Haensel, J. Meyer, and R. Schaeffer, Nucl. Phys. A **635**, 231 (1998).
[39] J. M. Lattimer and M. Prakash, Astroph. J. **550**, 426 (2001).
[40] Y. M. Wen and D. H. Wen, Phys. Rev. C **95**, 065804 (2017).
[41] I. Bombaci and U. Lombardo, Phys. Rev. C **44**, 1892 (1991).
[42] B. A. Li, L. W. Chen, and C. M. Ko, Phys. Rep. **464**, 113 (2008).
[43] N. B. Zhang, B. A. Li, and J. Xu, Astrophys. J. **859**, 90 (2018).